# Ultraviolet Photoelectron Spectrum of $NO_2^-$

**Kent M. Ervin, Joe Ho, and W. C. Lineberger***

*Department of Chemistry and Biochemistry, University of Colorado, and Joint Institute for Laboratory Astrophysics, University of Colorado and National Bureau of Standards, Boulder, Colorado 80309*
*(Received: January 21, 1988; In Final Form: February 23, 1988)*

The 351.1-nm (3.532-eV) photoelectron spectrum of the nitrite anion ($NO_2^-$) is reported. The electron affinity of $NO_2$ is found to be 2.273 ± 0.005 eV, which leads to the heat of formation $\Delta_f H_0°(NO_2^-) = -183.4 \pm 0.9$ kJ/mol (−43.8 ± 0.2 kcal/mol). Vibrational progressions of the symmetric stretch and bending modes of nitrogen dioxide, $NO_2(\tilde{X}^2A_1)$, are observed up to 8000 $cm^{-1}$ above the ground state. Observed fundamental vibrational frequencies of $NO_2^-$ are $\nu_1 = 1284 \pm 30$ $cm^{-1}$ (symmetric stretch) and $\nu_2 = 776 \pm 30$ $cm^{-1}$ (bend). The vibrational band intensities are modeled by using a Franck–Condon analysis which explicitly treats the Duschinsky rotation of the normal coordinates between the anion and the neutral molecule. This analysis provides an estimate of the equilibrium geometry of the anion: $r_e(N-O) = 1.25 \pm 0.02$ Å and $\alpha_e(O-N-O) = 117.5 \pm 2°$.

## I. Introduction

The spectroscopy of $NO_2$ is notoriously complex and has provided a challenge for several generations of scientists, among them Professor E. K. C. Lee,[1] in whose memory this Special Issue is dedicated. Two "spectral atlases"[2,3] of $NO_2$ have been published which catalog thousands of vibrational and rotational lines in the visible spectrum. Much of the complexity of this system arises from interactions among three low-lying electronically excited states and the ground state. Various perturbation mechanisms produce a much greater density of rotational and vibrational lines than would otherwise be expected for a triatomic species. Interest in $NO_2$ is fueled by a desire to understand these perturbations on a fundamental level, as well as by its importance in the Earth's atmosphere. The atlas of Hsu, Monts, and Zare[2] includes a review of theoretical aspects of $NO_2$ and a historical perspective; Uehara and Sasada's atlas[3] contains a bibliography of the recent spectroscopic literature.

The anion $NO_2^-$ has been studied using photodetachment threshold techniques by Herbst et al.[4] and by Woo et al.[5] In these works, the threshold behavior of the photodetachment cross section was modeled by using Franck–Condon analyses to obtain estimates of the electron affinity of $NO_2$, given in Table I. These electron affinities are in general agreement with values obtained from electron-transfer reaction studies[6-8] and a theoretical value,[9] also shown in Table I. Woo et al.[5] also obtained geometries for the anion from the photodetachment threshold analysis. The vibrational spectrum of gas-phase $NO_2^-$ has not been observed, but vibrational frequencies (Table II) of the anion in crystalline,[10-12] aqueous,[13] and argon matrix[14] environments are known. Several ab initio calculations of $NO_2^-$ have also been reported.[9,15-17]

In this work, we report the ultraviolet photoelectron spectrum of $NO_2^-(\tilde{X}\ ^1A_1)$. The spectrum is obtained by measuring the kinetic energy of photodetached electrons from the process

$$NO_2^-(v'') + h\nu \rightarrow NO_2(v') + e^-$$

**TABLE I: Adiabatic Electron Affinity of $NO_2$**

| EA($NO_2$), eV | method | ref |
|---|---|---|
| 2.273 ± 0.005 | photoelectron spectroscopy | this work |
| 2.275 ± 0.025 | photodetachment threshold | 5 |
| 2.36 ± 0.1 | photodetachment threshold | 4 |
| 2.30 ± 0.1 | charge-transfer equilibria | 6 |
| 2.28 ± 0.10 | endoergic charge transfer | 7 |
| 2.38 ± 0.06 | exoergic charge transfer | 8 |
| 2.25 | ab initio SCF | 9 |

where $v''$ and $v'$ denote the vibrational states of the ionic and neutral species. The adiabatic electron affinity of $NO_2$ is determined and the vibrational spectrum of $NO_2(\tilde{X}\ ^2A_1)$ is observed in the region within 1 eV of its ground vibrational level. A Franck–Condon analysis of the vibrational intensities provides an estimate of the equilibrium geometry of the anion.

## II. Experimental Methods

*A. Photoelectron Spectrometer.* The photoelectron spectrometer used in these experiments has been described in detail previously.[18] In brief, negative ions are produced in a flowing afterglow source, accelerated and focused into an ion beam, mass selected with a Wien velocity filter, and finally crossed with a continuous laser beam of fixed photon energy. Photodetached electrons are extracted perpendicularly to the ion and laser beams, and their kinetic energies are determined with a hemispherical electrostatic energy analyzer. Transition energies between the initial state of the anion and the final state of the neutral molecule are obtained as the difference between the photon energy and the measured electron kinetic energy.

For this work, the electron kinetic energies are calibrated on the $^3P_2 \leftarrow {}^2P_{3/2}$ and $^1D_2 \leftarrow {}^2P_{3/2}$ transitions[19] in the photodetachment of $S^-$, using EA(S) = 2.277 12 eV.[20] Measured kinetic energies of peaks in the spectrum have an uncertainty of ±0.005 eV. The instrumental energy resolution is 9 meV fwhm. The relative peak intensities above 0.5 eV have an uncertainty of less than 20%, as has been verified by examining the Franck–Condon intensity profiles of the $\tilde{X}\ ^3\Sigma_g^-$ (0.0-eV), a $^1\Delta_g$ (0.982-eV), and b $^1\Sigma_g^+$ (1.636-eV) states[21] of $O_2$ in the photoelectron spectrum of $O_2^-$ [EA($O_2$) = 0.440 ± 0.008 eV].[22] These well-characterized

(1) Uselman, W. M.; Lee, E. K. C. *Ber. Bunsen-Ges. Phys. Chem.* **1974**, *78*, 203; *Chem. Phys. Lett.* **1975**, *30*, 212; *J. Chem. Phys.* **1976**, *65*, 1948; *J. Chem. Phys.* **1976**, *64*, 3457.
(2) Hsu, D. K.; Monts, D. L.; Zare, R. N. *Spectral Atlas of Nitrogen Dioxide 5530 Å to 6480 Å*; Academic: New York, 1978.
(3) Uehara, K.; Sasada, H. *High Resolution Spectral Atlas of Nitrogen Dioxide 559–597 nm*; Springer: Berlin, 1985.
(4) Herbst, E.; Patterson, T. A.; Lineberger, W. C. *J. Chem. Phys.* **1974**, *61*, 1300.
(5) Woo, S. B.; Helmy, E. M.; Paszek, A. P. *Phys. Rev. A* **1981**, *24*, 1380.
(6) Chowdhury, S.; Heinis, T.; Grimsrud, E. P.; Kebarle, P. *J. Phys. Chem.* **1986**, *90*, 2747. Kebarle, P.; Chowdhury, S. *Chem. Rev.* **1987**, *87*, 513.
(7) Hughes, B. M.; Lifshitz, C.; Tiernan, T. O. *J. Chem. Phys.* **1972**, *59*, 3162.
(8) Dunkin, D. B.; Fehsenfeld, F. C.; Ferguson, E. E. *Chem. Phys. Lett.* **1972**, *15*, 257.
(9) Anderson, E.; Simons, J. *J. Chem. Phys.* **1977**, *66*, 2427.
(10) Gotberg, K. E.; Tinti, D. S. *Chem. Phys.* **1985**, *96*, 109.
(11) Fadini, A.; Klopsch, A.; Busch, B. *J. Mol. Struct.* **1980**, *64*, 201.
(12) Kato, R.; Rolfe, J. *J. Chem. Phys.* **1967**, *47*, 1901.
(13) Weston, R. E., Jr.; Brodasky, T. F. *J. Chem. Phys.* **1957**, *27*, 683.
(14) Jacox, M. E. *J. Phys. Chem. Ref. Data* **1984**, *18*, 945.
(15) Handy, N. C.; Goddard, J. D.; Schaefer, H. F., III *J. Chem. Phys.* **1979**, *71*, 426.
(16) Goddard, J. D.; Klein, M. L. *Phys. Rev. A* **1983**, *28*, 1141.
(17) Harrison, R. J.; Handy, N. C. *Chem. Phys. Lett.* **1983**, *97*, 410.
(18) Leopold, D. G.; Murray, K. K.; Stevens-Miller, A. E.; Lineberger, W. C. *J. Chem. Phys.* **1985**, *83*, 4849.
(19) Moore, C. E. *Atomic Energy Levels*; *Natl. Stand. Ref. Data Serv. Circ.* 1948, *no.* 467.
(20) Hotop, H.; Lineberger, W. C. *J. Phys. Chem. Ref. Data* **1985**, *14*, 731.

0022-3654/88/2092-5405$01.50/0 

**TABLE II: Vibrational Constants ($cm^{-1}$)**

| | $\omega_1^0$ | $\omega_2^0$ | $\omega_3^0$ | $x_{11}$ | $x_{22}$ | $x_{12}$ | ref |
|---|---|---|---|---|---|---|---|
| $NO_2$ | 1325.33 ± 0.06 | 750.14 ± 0.02 | 1633.86 ± 0.05 | −5.471 ± 0.032 | −0.469 ± 0.015 | −6.433 ± 0.023 | 33 |
| $NO_2$ | 1316.4 ± 9.2 | 748.0 ± 4.2 | | −3.1 ± 2.6 | −0.59 ± 0.44 | −2.1 ± 1.3 | this work[a] |
| $NO_2^-$[b] | 1284 ± 30 | 776 ± 30 | | | | | this work |
| $NO_2^-(Ar)$[b,c] | | | 1244 | | | | 14 |
| $NO_2^-(KBr)$[b,d] | 1316.2 | 798.1 | 1275.0 | | | | 12 |
| $NO_2^-(NaNO_2)$[e] | 1330[b] | 829.7 | 1242[b] | | −0.77 | −6.7 | 10 |
| $NO_2^-(aq)$[b] | 1332 | 821 | 1240 | | | | 13 |

[a] Linear regression fit to eq 2 with observed peak positions given in Table III. Uncertainties are two standard deviations. [b] Fundamental frequencies, $\nu_i = \omega_i + x_{ii}$. [c] Argon matrix. [d] $NO_2^-$ in dilute concentration in crystalline KBr. [e] Crystalline $NaNO_2$.

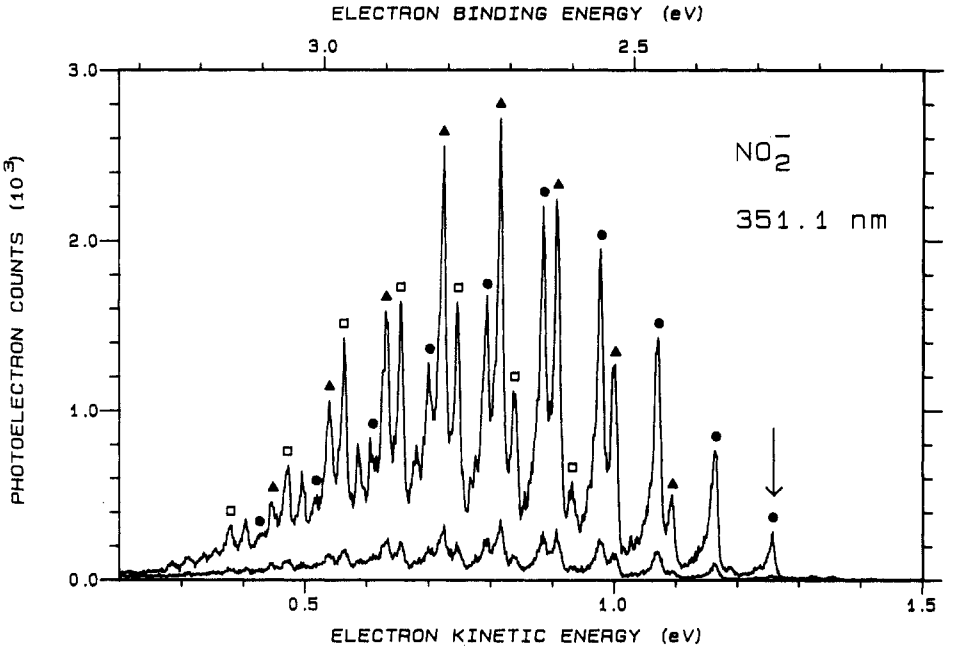


**Figure 1.** Photoelectron spectrum of $NO_2^-$ obtained with 351.1-nm photons. The electron binding energy, upper scale, is the photon energy minus the measured electron kinetic energy, lower scale. The upper trace represents a laser polarization parallel to the electron collector direction, and the lower trace had polarization perpendicular to the collector direction. The origin peak is indicated by an arrow. Vibrational assignments are indicated by symbols above the transitions: the $1_0^0 2_0^n$ bend mode overtone progression is marked by circles, the $1_0^1 2_0^n$ progression is marked by triangles, and the $1_0^2 2_0^n$ progression is marked by squares.

species have overlapping vibrational progressions in the kinetic energy range of 0.5–3.0 eV. Diagnostic spectra of other species indicate that the sensitivity of the electron analyzer declines slowly below 0.5 eV and more rapidly below 0.2 eV.

*B. Laser System.* In the past, the photoelectron spectrometer has operated primarily on the blue and green (2.4–2.6 eV) lines of an argon ion laser. Intracavity operation provides up to 100 W of circulating power focused to 0.01 $mm^2$ at the intersection with the ion beam. While use of the near-ultraviolet lines of the laser in the intracavity mode is possible,[23] the low gain of these lines results in a power loss of more than an order of magnitude and low signal-to-noise levels make routine operation infeasible. We have recently implemented an external cavity buildup system which provides for operation on the 351.1-nm (3.532-eV) Ar III line at higher power levels. Details of the optics system will be presented elsewhere, with only a brief description here. An internal solid etalon is placed in the laser resonator to provide single mode operation, and an external prism selects the 351.1-nm line. This single-frequency laser light passes through a mode-matching telescope and is injected into an external optical resonator cavity (near concentric). The focal point of the external cavity is at the point of intersection with the ion beam. The mirrors (99.6% reflectivity) of this cavity form the vacuum wall of the photoelectron spectrometer. Frequency matching of the laser and external cavities is accomplished via an acoustooptic frequency modulator, piezoelectric controlled mirrors on both cavities, and an electronic feedback system. Because the external cavity has low losses and is continuously pumped by the input laser beam, substantial build-up of the power is possible.[24] We obtain a buildup of 200 (the ratio of the laser power inside the cavity to the incident power) on a routine basis, which for input powers of 150–200 mW provides powers of 30–40 W in the interaction region. Further increases in the power level are possible by use of higher reflectivity mirrors and by improvements in the output power of the argon ion laser. The optical isolation of the laser cavity and the lack of polarization sensitive elements in the external buildup cavity mean that the polarization of the laser light in the interaction region can be rotated conveniently by use of a $\lambda/2$ plate. This capability permits studies of the angular intensity distributions of the photodetached electrons, which provides information about the electronic nature of the transition.[25-27]

*C. Ion Production.* $NO_2^-$ is a very stable anion, as indicated by the high electron affinity of the neutral, $EA(NO_2) \approx 2.3$ eV (see Table I), and is frequently observed as an impurity in the mass spectrum from the flowing afterglow ion source. In this work, $NO_2^-$ is produced by leaking air into the flow tube of the ion source, either upstream or downstream of a microwave discharge in a helium flow. $NO_2^-$ ion currents of 500–700 pA at the interaction region are obtained when air is admitted upstream of the discharge; 100–200 pA currents are observed when the in-

(21) Huber, K. P.; Herzberg, G. *Molecular Spectra and Molecular Structure. IV. Constants of Diatomic Molecules*; Van Nostrand Reinhold: New York, 1979.
(22) Celotta, R. J.; Bennett, R. A.; Hall, J. L.; Siegel, M. W.; Levine, J. *Phys. Rev. A* **1972**, *6*, 631.
(23) Engelking, P. C.; Lineberger, W. C. *J. Am. Chem. Soc.* **1979**, *101*, 5569.
(24) Siegman, A. E. *Lasers*; University Science Books: Mill Valley, CA, 1986; p 413 ff.
(25) Cooper, J.; Zare, R. N. *J. Chem. Phys.* **1968**, *48*, 942. Hall, J. L.; Siegel, M. W. *J. Chem. Phys.* **1968**, *48*, 943.
(26) Chandra, N. *Phys. Rev. A* **1987**, *36*, 3163.
(27) Katamatsu, S.; Shiromaru, H.; Mitani, K.; Iwata, S.; Kimura, K. *Chem. Phys.* **1982**, *69*, 423.

**TABLE III: Vibrational Assignments**

| assignment | | | | | | rel intensity | |
|---|---|---|---|---|---|---|---|
| $v_1'$ | $v_2'$ | ← | $v_1''$ | $v_2''$ | $G_0$,[a] $cm^{-1}$ | obsd[b] | FCF[c] |
| 0 | 0 | | 0 | 0 | 0 | 1 | 1.0 |
| 0 | 1 | | 0 | 0 | 749 | 3 | 3.5 |
| 1 | 0 | | 0 | 0 | 1301 | 2 | 1.5 |
| 0 | 2 | | 0 | 0 | 1501 | 6 | 6.1 |
| 1 | 1 | | 0 | 0 | 2059 | 5 | 4.9 |
| 0 | 3 | | 0 | 0 | 2241 | 6 | 6.9 |
| 2 | 0 | | 0 | 0 | 2611 | 1 | 1.1 |
| 1 | 2 | | 0 | 0 | 2805 | 8 | 8.2 |
| 0 | 4 | | 0 | 0 | 2990 | 6 | 5.8 |
| 2 | 1 | | 0 | 0 | 3362 | 4 | 3.5 |
| 1 | 3 | | 0 | 0 | 3545 | 10 | 9.0 |
| 0 | 5 | | 0 | 0 | 3726 | 3 | 3.8 |
| 2 | 2 | | 0 | 0 | 4110 | 5 | 5.7 |
| 1 | 4 | | 0 | 0 | 4292 | 7 | 7.2 |
| 0 | 6 | | 0 | 0 | 4463 | 2 | 2.1 |
| 3 | 1 | | 0 | 0 | 4667 | 2 | 1.7 |
| 2 | 3 | | 0 | 0 | 4845 | 6 | 6.0 |
| 1 | 5 | | 0 | 0 | 5033 | 5 | 4.6 |
| 0 | 7 | | 0 | 0 | 5213 | 0.9 | 1.0 |
| 3 | 2 | | 0 | 0 | 5395 | 3 | 2.7 |
| 2 | 4 | | 0 | 0 | 5587 | 5 | 4.6 |
| 1 | 6 | | 0 | 0 | 5771 | 2 | 2.4 |
| 0 | 8 | | 0 | 0 | 5952 | 0.3 | 0.4 |
| 3 | 3 | | 0 | 0 | 6135 | 2 | 2.7 |
| 2 | 5 | | 0 | 0 | 6331 | 2 | 2.8 |
| 1 | 7 | | 0 | 0 | 6517 | 1 | 1.1 |
| 0 | 9 | | 0 | 0 | 6687 | 0.1 | 0.1 |
| 3 | 4 | | 0 | 0 | 6875 | 1 | 2.0 |
| 2 | 6 | | 0 | 0 | 7075 | 0.8 | 1.4 |
| 0 | 0 | | 1 | 0 | −1284 | | |
| 0 | 2 | | 2 | 0 | −1050 | | |
| 0 | 0 | | 0 | 1 | −776 | | |
| 0 | 1 | | 1 | 0 | −532 | | |
| 0 | 2 | | 1 | 0 | 212 | | |
| 1 | 0 | | 0 | 1 | 547 | | |
| 0 | 3 | | 1 | 0 | 940 | | |

[a] Measured peak positions. ±20-$cm^{-1}$ uncertainty, ±30-$cm^{-1}$ uncertainty for hot bands. [b] Observed intensities, relative to origin. [c] Franck–Condon factors calculated by method IV (see text), relative to origin.

jection point is downstream of the discharge. The photoelectron spectra demonstrate that ions from upstream injection are vibrationally hotter than those formed downstream. This phenomenon results from the more vigorous conditions in the discharge compared to the low-density plasma downstream and, in addition, from the weak vibrational quenching rate by collisions with the helium buffer gas. Rotational energy is more easily thermalized by collisions in the helium flow. A case where this can be shown experimentally is in the photoelectron spectrum of $OH^-$, where partially resolved rotational structure[28,29] provides a rotational "thermometer" of the anions. Our measurements[30] for $OH^-$ indicate a 315 ± 20 K rotational temperature for ions made in the flowing afterglow with a microwave discharge under a variety of source conditions.

## III. Results and Analysis

*A. Photoelectron Spectrum.* The higher photon energy afforded by the UV laser system has allowed us to obtain the photoelectron spectrum of $NO_2^-$, where it had not been observable previously with 488-nm excitation. The high electron affinity of $NO_2$, combined with unfavorable Franck–Condon factors near the threshold for photodetachment, has prevented measurement of the photoelectron spectrum with visible lasers.

Figure 1 shows the photoelectron spectrum of $NO_2^-$ with a 3.532-eV photon energy (351.1 nm) over the electron kinetic energy range 0.2–1.5 eV. Scans at higher kinetic energy showed no indication of additional transitions. The observed width of the peaks is 16 meV fwhm, a combination of the 9 meV fwhm instrumental resolution and rotational broadening.

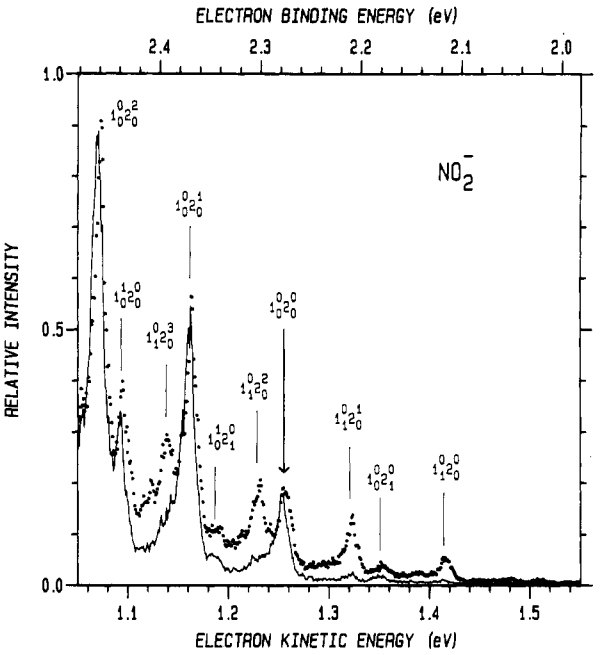


**Figure 2.** Photoelectron spectra of $NO_2^-$ produced under different ion source conditions. The line shows the spectrum of anions with a vibrational temperature of 350 ± 50 K; the point shows 700 ± 100 K anions. The two spectra have been normalized for differences in the ion current, laser power, and collection time. The large arrow marks the vibrational origin peak. Vibrational assignments are indicated for prominent transitions.

The photoelectron spectrum shows extended progressions which may be identified with transitions of the two totally symmetric vibrational modes of $NO_2$, the $\nu_1$ symmetric stretch and the $\nu_2$ bend modes. The $\nu_3$ asymmetric stretch is not active because of symmetry considerations.[4] Vibrational assignments are indicated in Figure 1 and listed in Table III. The $1_0^0 2_0^0$ origin transition, whose assignment will be justified below, is shown by an arrow. The $\nu_2$ bend overtone progression, $1_0^0 2_0^n$, indicated in Figure 1, is identified by the ~750-$cm^{-1}$ spacing between the peaks, which corresponds to the known bend frequency of $NO_2$ (see Table II). Combination bands which correspond to progressions of the bend built upon one ($1_0^1 2_0^n$) or two ($1_0^2 2_0^n$) quanta in the symmetric stretch mode (~1320 $cm^{-1}$) can also be identified, as well as several peaks in the $1_0^3 2_0^n$ progression. The progressions in the bend mode are quite extended, with peak intensities between $3\nu_2$ and $4\nu_2$ and transitions observed up to $9\nu_2$, while the symmetric stretch progression peaks between $1\nu_1$ and $2\nu_1$.

*B. Polarization Dependence.* Two scans with different laser polarizations are shown in Figure 1: $\theta = 0°$ and $\theta = 90°$, where $\theta$ is the angle between the electric field vector and the ejected electron. The ratio of the intensities of the $\theta = 0°$ and $\theta = 90°$ scans is nearly constant over the range of the progression and is given by $\sigma(\theta=0°)/\sigma(\theta=90°) \approx 7.6$. From this value we can derive an approximate value for the anisotropy parameter, $\beta \approx 1.4$,[31] where $\beta$ is defined by the following relationship[25] for the angular distribution:

$$d\sigma/d\Omega = (\sigma_0/4\pi)[1 + \beta P_2(\cos\theta)] \quad (1)$$

Here $\sigma_0$ is the total photodetachment cross section and $P_2(\cos\theta) = (3\cos^2\theta - 1)/2$. Measurement of more precise values of $\beta$ would require observations at many polarization angles, which was not done. The approximately constant value of $\beta$ over the entire progression is consistent with all of the observed bands arising from a single electronic transition.[32] The anisotropy

(28) Beyer, F.; Frey, P.; Hotop, H. *Z. Phys. A* **1981**, *300*, 7.
(29) Schulz, P. A.; Mead, R. A.; Lineberger, W. C. *Phys. Rev. A* **1983**, *27*, 2229.
(30) Ervin, K. M.; Ho, J.; Lineberger, W. C., unpublished results.

(31) Zero-core-contribution calculations of the photodetachment cross section of $NO_2^-$ (Clodius, W. B.; Stehman, R. M.; Woo, S. B. *Phys. Rev. A* **1983**, *28*, 760) predict an anisotropy factor of $\beta = 0.25$–$0.75$, which would lead to the intensity ratio $\sigma(\theta=0°)/\sigma(\theta=90°) = 1.4$–$2.8$. This prediction is inconsistent with the present results. These calculations used the molecular geometries of Woo et al. (ref 5) as input data.

parameter is also expected to depend weakly on the kinetic energy of the ejected electron.[25,26]

*C. Origin Assignment.* In this section, we discuss information that supports our assignment of the vibrational origin peak, indicated by the vertical arrow in Figure 1. First, the electron kinetic energy (eKE) of the assigned origin peak is the highest among prominent observed transitions. Its value at the peak maximum, eKE = 1.256 eV, gives an approximate value for the electron affinity $EA(NO_2) = h\nu - eKE \approx 2.276$ eV (see below for experimental corrections to the electron affinity), which agrees well with values obtained by previous experiments, compared in Table I.

Second, spectra taken under different ion source conditions show that the assigned origin peak has a constant intensity relative to other peaks in the $NO_2$ progressions, while the intensities of *all* transitions observed at higher electron kinetic energy vary with source conditions. This is shown in Figure 2, which compares the origin region of the spectrum for ions produced downstream of the microwave discharge with the spectrum for ions produced in the discharge. In the latter case, the anions are vibrationally hot, as indicated by increases in the relative intensities of hot bands to the right of the origin and also by the appearance of several sequence bands to the left of the origin. Vibrational assignments of the hot bands and sequence bands are indicated in Figure 2 and Table III. The anion vibrational temperatures, estimated from the hot-band intensities, are 350 ± 50 and 700 ± 100 K for the two cases, respectively. Electronically excited states of the anion lie much higher in energy[15] and are not populated.

Third, the frequency spacings between the transitions in the symmetric stretch and bend progressions, 1320 ± 20 and 750 ± 20 $cm^{-1}$, respectively, agree well with the known frequencies of $NO_2$. However, the frequency spacings between the assigned origin and peaks with similar spacings to higher kinetic energy, 1284 ± 30 and 776 ± 30 $cm^{-1}$, differ from the neutral $NO_2$ frequencies. These peaks may be assigned to transitions that originate from anions with one quantum of vibrational excitation in the symmetric stretch or bend modes, $1_1^0 2_0^0$ and $1_0^0 2_1^0$, respectively. Assignments of additional hot bands and sequence bands are given in Table III and Figure 2. Final confirmation of the vibrational assignments will be provided by the Franck–Condon analysis of the band intensities, discussed below.

*D. Vibrational Constants.* Vibrational constants for $NO_2$ are obtained by a linear regression fit of the observed transition energies to the expression

$$G_0(v_1,v_2) = \omega_1^0 v_1 + \omega_2^0 v_2 + x_{11}v_1^2 + x_{22}v_2^2 + x_{12}v_1v_2 \quad (2)$$

Table III lists the measured transition energies, which represent averages of peak positions obtained from several independent scans. The calculated vibrational constants, presented in Table II, reproduce all measured peak positions within their ±20-$cm^{-1}$ uncertainty. Table II also shows the constants obtained from high-resolution spectroscopic results of Lafferty and Sams.[33] Our values for the vibrational constants correspond to the peaks of the rotational contours, while Lafferty and Sam's values are for rotationless transitions. Nevertheless, agreement is quite good, except for the anharmonicity constants involving the $\nu_1$ mode, for which levels only up to $3\nu_1$ are observed in the present work.

Fundamental frequencies for the anion can be determined from hot-band positions. Again, two modes are observed: $\nu_1$ = 1284 ± 30 $cm^{-1}$ and $\nu_2$ = 776 ± 30 $cm^{-1}$. We do not attempt to obtain anharmonicities since few transitions from higher vibrational levels of the anion are observed. The symmetric stretch frequency is 3% smaller for the anion than the neutral, while the bend frequency is 3% larger (see Table II).

*E. Electron Affinity and Thermochemistry.* The adiabatic electron affinity may differ from the value obtained from the electron kinetic energy at the maximum of the origin peak because of unresolved sequence bands and rotational broadening. For the scans with low anion vibrational temperatures, the intensities of sequence bands near the origin, e.g., $1_0^0 2_1^1$, and $1_1^1 2_0^0$, are not large enough to shift the observed peak position significantly. This conclusion is based on Franck–Condon intensity simulations, discussed below. The rotational band shift[34] is determined by modelling the rotational contours, for which $NO_2$ and $NO_2^-$ are approximated as prolate tops. The band contours of the $1_0^0 2_0^0$ and $1_0^0 2_0^1$ transitions, which are relatively well isolated from other peaks, could be matched with an anion rotational temperature of 300 K and a Q-branch intensity of 2 relative to the P- and R-branches, convoluted with the measured instrumental resolution of 9 meV fwhm. This contour is shown in the inset of Figure 3. Other combinations of the temperature and Q-branch intensity could fit the peaks, but the derived band shift correction, +3 meV, is insensitive to these parameters. Including this correction, the rotationless origin is eKE = 1.259 ± 0.005 eV, which results in our final value for the electron affinity, $EA(NO_2)$ = 2.273 ± 0.005 eV. This agrees well with previous experimental and theoretical values, which are compared in Table I.

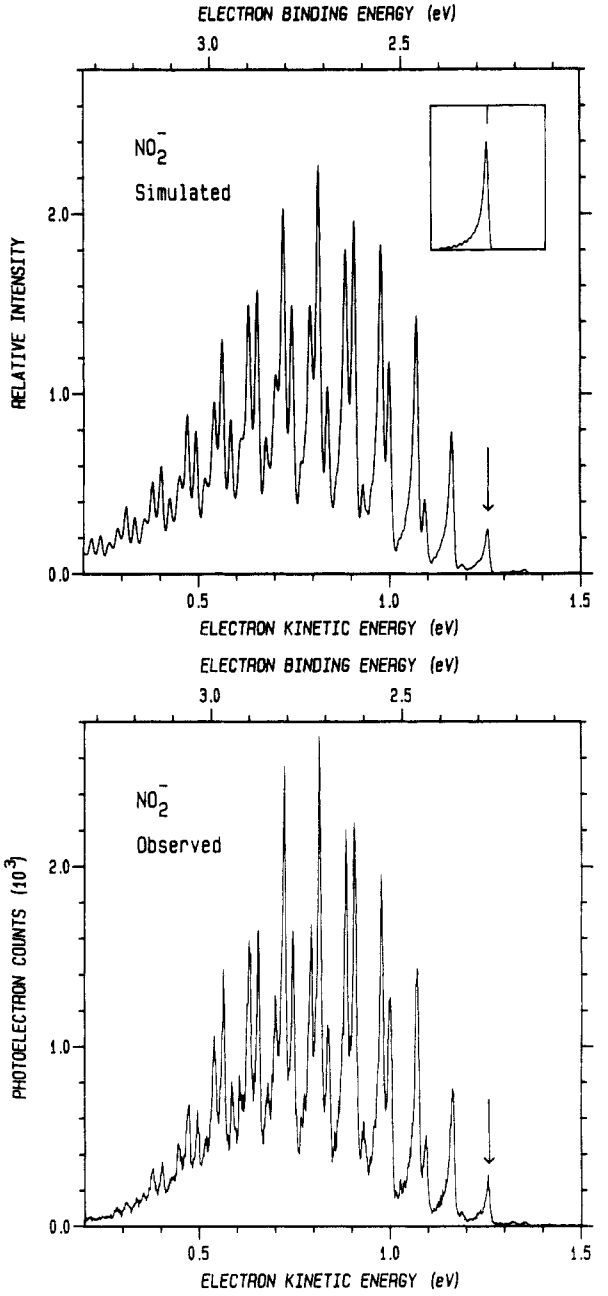


**Figure 3.** Comparison of the experimental photoelectron spectrum (lower plot) with the Franck–Condon simulation (upper plot), calculated by method IV (see text). The inset shows the shape of the simulated rotational contour. Arrows mark the origin peak.

The heat of formation of $NO_2^-$ may be derived from

$$\Delta_f H_0^\circ(NO_2^-) = \Delta_f H_0^\circ(NO_2) - EA(NO_2) \quad (3)$$

(32) Cox, P. A.; Orchard, F. A. *Chem. Phys. Lett.* **1970**, *7*, 273. Cox, P. A.; Evans, S.; Orchard, A. F. *Chem. Phys. Lett.* **1972**, *13*, 386.

(33) Lafferty, W. J.; Sams, R. L. *J. Mol. Spectrosc.* **1977**, *66*, 478.

(34) Engelking, P. C. *J. Phys. Chem.* **1986**, *90*, 4544.

**TABLE IV: Molecular Geometries**

| species | method[a] | $r_e$, Å | $\alpha$, deg | ref |
|---|---|---|---|---|
| $NO_2$ | S | 1.19389 ± 0.00004 | 133.857 ± 0.003 | 40 |
| | | Experiment | | |
| $NO_2^-$ | PES | 1.25 ± 0.02 | 117.5 ± 2 | this work |
| $NO_2^-$ | PDT 1[b] | 1.15 ± 0.02 | 119.5 ± 1.0 | 5 |
| $NO_2^-$ | PDT 2[b] | 1.25 | 116 | 5 |
| $NO_2^-$(cryst) | neutron diff | 1.240 ± 0.003 | 114.9 ± 0.5 | 51 |
| | | Theory | | |
| $NO_2^-$ | SCF | 1.226 | 117.42 | 16 |
| $NO_2^-$ | SCF | 1.223 ± 0.005 | 117.1 ± 1 | 17 |
| $NO_2^-$ | SCF | 1.26 | 118 | 9 |

[a] S, spectroscopic; PES, photoelectron spectroscopy; PDT, photodetachment threshold; SCF, ab initio self-consistent field. [b] Two possible fits found by Woo et al. (ref 5). Woo et al. adopted PDT 1, but the present work indicates that PDT 2 is more accurate (see text).

Using $\Delta_f H_0°(NO_2) = 35.93 \pm 0.8$ kJ/mol,[35] we obtain $\Delta_f H_0°(NO_2^-) = -183.4 \pm 0.9$ kJ/mol ($-43.8 \pm 0.2$ kcal/mol).[36] The energy for $NO_2^-$ dissociating to $O^-$ and NO may be determined from

$$D_0°(O^-\text{–}NO) = EA(NO_2) - EA(O) + D_0°(NO\text{–}O) \quad (4)$$

Using the present value for $EA(NO_2)$, $EA(O) = 1.461125$ eV,[20] and $D_0°(O\text{–}NO) = 300.64 \pm 0.8$ kJ/mol ($3.12 \pm 0.01$ eV),[35] eq 4 gives $D_0°(O^-\text{–}NO) = 379.4 \pm 0.9$ kJ/mol ($3.93 \pm 0.01$ eV). We may also derive the gas-phase acidity of nitrous acid, the enthalpy for the reaction $HONO \rightarrow H^+ + NO_2^-$, from the relation

$$\Delta H_a°(HONO) = D_0°(H\text{–}ONO) + IP(H) - EA(NO_2^-)$$

Using $D_0°(H\text{–}ONO) = 324.6 \pm 1.6$ kJ/mol for *trans*-HONO,[35] $IP(H) = 1312.05 \pm 0.04$ kJ/mol,[35] and the present value for $EA(NO_2)$, we obtain $\Delta H_a°(HONO) = 1417.4 \pm 1.7$ kJ/mol ($338.8 \pm 0.4$ kcal/mol) at 0 K.

## IV. Discussion

*A. Qualitative Interpretation.* All of the observed vibrational structure in the photoelectron spectrum is accounted for by progressions in the $\nu_1$ symmetric stretch and $\nu_2$ bend vibrational modes of $NO_2(\tilde{X}\,^2A_1)$. Recent ab initio calculations[37] place the energy of the $\tilde{A}\,^2B_2$ state 0.92 eV above the ground state and the $\tilde{B}\,^2B_1(^1\Pi_u)$ state, which is degenerate with $\tilde{X}\,^2A_1$ in the linear configuration, at 1.91 eV. The vibrational structure of the molecule in the region of the present observations, which is below the level of these excited states, does not exhibit the complexity seen at higher energies.

The intensity distribution of the vibrational transitions is governed by the Franck–Condon overlap of the vibrational wave functions of the initial ($NO_2^-$) and final ($NO_2$) states in the photodetachment process. The extended progression of the bend mode in $NO_2$ indicates that there is a large change in the bond angle between the anion and the neutral. The progression in the symmetric stretch mode indicates that there is also a significant change in the bond length.

Molecular orbital considerations, in particular the Mulliken–Walsh model,[38] may be used to determine the direction of the geometry changes between the anion and neutral. Buenker and Peyerimhoff[39] have reviewed the theoretical basis of the Walsh rules[38] for changes in bond angle according to molecular orbital occupancy and have extended them to include how molecular orbital occupancies affect bond lengths. $NO_2$ has 17 valence electrons with the molecular orbital configuration $...(1a_2)^2(4b_2)^2(6a_1)^1$. It is bent, with bond angle $\alpha' = 134°$ and bond length $r' = 1.194$ Å.[40] According to the Walsh rules, addition of an electron into the $6a_1$ molecular orbital to form the anion will lead to a substantial decrease in the bond angle. On this basis, we may conclude that the bond angle of $NO_2^-$ is smaller than that of $NO_2$. This is consistent with $NO_2^-$ in crystalline environments, where it is known to be much more strongly bent than is $NO_2$ (see Table IV). As discussed by Buenker and Peyerimhoff,[39] addition of an electron to the $6a_1$ molecular orbital will also tend to increase the N–O bond length. This increase results from the antibonding nature of the $6a_1$ molecular orbital with respect to N–O. Therefore, the N–O bond length in $NO_2^-$ is expected to be longer than in $NO_2$.

These expectations for the change in geometry are supported by the observed changes in vibrational frequencies upon removal of the electron. The $\nu_1$ symmetric stretch frequency is smaller for $NO_2^-$ than for $NO_2$, consistent with a weaker, longer N–O bond in the anion. The $\nu_2$ bend frequency changes in the opposite direction, consistent with stronger interaction between the oxygen atoms and smaller bond angle. While a possible counter argument is that $D_0°$ ($O^-$–NO) = 3.93 eV is larger than $D_0°$ (O–NO) = 3.12 eV, the asymmetric bond dissociation limit should have little correlation with equilibrium force constants or bond lengths.

*B. Franck–Condon Analysis.* Quantitative information about the change in geometry of $NO_2^-$ upon electron detachment may be obtained by a Franck–Condon analysis of the relative intensities of the vibrational transitions. The geometry and vibrational structure of $NO_2$ are well established; we aim to determine the geometry of $NO_2^-$ using only experimental data. Since two modes are active and there is a large geometry change, assumptions often made in the analysis of photoelectron spectra (e.g., local mode and single-dimension approximations) are not valid. Therefore, we will first briefly review the theory of Franck–Condon intensity factors.

*1. Theoretical Framework.* The Franck–Condon overlap integral is given by[41,42]

$$C(v',v'') = \int \psi_{v'}(\mathbf{Q}')\psi_{v''}(\mathbf{Q}'')\, d\mathbf{Q}' \quad (5)$$

where $\psi'_{v'}(\mathbf{Q}')$ is the vibrational wave function of the neutral in quantum state $v' = (v_1',v_2',v_3')$ as a function of the (mass-weighted) normal coordinates of the neutral $\mathbf{Q}'$ and $\psi''_{v''}(\mathbf{Q}'')$ is the corresponding vibrational wave function of the anion in terms of its normal coordinates $\mathbf{Q}''$. Throughout, single primes refer to the upper, final state ($NO_2$) and double primes refer to the lower, initial state ($NO_2^-$). The relative intensity of a vibrational transition is given by $[C(v',v'')]^2$, referred to as the Franck–Condon factor (FCF), in the approximation that the electronic transition probability is constant over the range of the vibrational overlap. This approximation should be valid since the electronic transition probability is a slowly varying function of the nuclear coordinates and because most of the observed transitions originate from the ground vibrational state of the anion, which restricts the range of significant overlap. Making the further approximation that the normal modes in each state are uncoupled, the wave functions are given by the product of one-dimensional wave functions in each normal coordinate

$$\psi_v(\mathbf{Q}) = \psi_{v_1}(Q_1)\,\psi_{v_2}(Q_2)\,\psi_{v_3}(Q_3) \quad (6)$$

In order to carry out the integration in eq 5, the wave functions must be expressed in terms of the same coordinates for both states. The transformation between the normal coordinates of the two states is given by

$$\mathbf{Q}'' = \mathbf{J}''\mathbf{Q}' + \mathbf{K}'' \quad (7)$$

where $\mathbf{K}'' = (\Delta Q_1'',\Delta Q_2'',\Delta Q_3'')$ is the vector of geometry displacements given in the basis of normal coordinates of the anion. $\mathbf{J}''$ is the Duschinksy[42,43] rotation matrix, defined by

(35) Chase, M. W., Jr.; Davies, C. A.; Downey, J. R., Jr.; Frurip, D. J.; McDonald, R. A.; Syverud, A. N. *JANAF Thermochemical Tables*, 3rd ed.; *J. Phys. Chem. Ref. Data, Suppl.* **1987**, *14(1)*.

(36) This heat of formation represents a correction of the value adopted in the JANAF Thermochemical Tables (ref 35), $\Delta_f H_0°(NO_2^-) = -193.73 \pm 5.8$ kJ/mol ($-46.30 \pm 1.4$ kcal/mol), which is based on $EA(NO_2) = 2.38 \pm 0.06$ eV from charge-transfer reaction studies (ref 8).

(37) Hirsch, G.; Buenker, R. J. *Can. J. Chem.* **1985**, *63*, 1542.

(38) Walsh, A. D. *J. Chem. Soc.* **1953**, 2260, 2266.

(39) Buenker, R. J.; Peyerimhoff, S. D. *Chem. Rev.* **1974**, *74*, 127.

(40) Morino, Y.; Tanimoto, M.; Saito, S.; Hirota, E.; Awata, R.; Tanaka, T. *J. Mol. Spectrosc.* **1983**, *98*, 331.

(41) Hutchisson, E. *Phys. Rev.* **1930**, *36*, 410; *Phys. Rev.* **1931**, *37*, 45.

(42) Sharp, T. E.; Rosenstock, H. M. *J. Chem. Phys.* **1964**, *41*, 3453. See also corrections in the Appendix of: Botter, R.; Dibeler, V. H.; Walker, J. A., Rosenstock, H. M. *J. Chem. Phys.* **1966**, *44*, 1271.

(43) Duschinsky, F. *Acta Physicochim. URSS* **1937**, *7*, 551.

$$\mathbf{J}'' = \tilde{\mathbf{L}}''\mathbf{L}' \tag{8a}$$

and

$$\mathbf{q}' = \mathbf{L}'\mathbf{Q}' \quad \text{and} \quad \mathbf{q}'' = \mathbf{L}''\mathbf{Q}'' \tag{8b}$$

where the columns of $\mathbf{L}$ are the eigenvectors for the normal coordinates $\mathbf{Q}$ in the basis of mass-weighted Cartesian displacement coordinates $\mathbf{q}$, and $\tilde{\mathbf{L}}$ is the transpose of $\mathbf{L}$. $\mathbf{L}'$ and $\mathbf{L}''$ may be obtained by a normal-coordinate analysis from the equilibrium geometry and force constants. The displacement vector $\mathbf{K}'$ in terms of the normal coordinates of the neutral is given by[44]

$$\mathbf{K}' = -\tilde{\mathbf{J}}''\mathbf{K}'' \tag{9}$$

With these definitions, $\mathbf{J}''$ is a unitary matrix and the Eckart condition[45,46] is satisfied, i.e., eq 7 does not introduce any translation or rotation of the molecule.

Symmetry considerations simplify the normal-coordinate transformation given by eq 7. The matrix $\mathbf{J}''$ factors into blocks corresponding to the totally symmetric ($\nu_1$ and $\nu_2$) and non-totally symmetric ($\nu_3$) vibrational modes. The two symmetric coordinates, $Q_1$ and $Q_2$, are related by a simple rotation between the two states. In addition, the displacement in non-totally symmetric modes is identically zero, i.e., $K_3 = 0$. For a bent symmetric triatomic molecule, therefore, eq 7 may be represented explicitly by

$$\begin{pmatrix} Q_1'' \\ Q_2'' \end{pmatrix} = \begin{pmatrix} \cos\phi & -\sin\phi \\ \sin\phi & \cos\phi \end{pmatrix}\begin{pmatrix} Q_1' \\ Q_2' \end{pmatrix} + \begin{pmatrix} \Delta Q_1'' \\ \Delta Q_2'' \end{pmatrix} \tag{10a}$$

and

$$Q_3'' = Q_3' \tag{10b}$$

Thus, the Franck–Condon factors are specified completely by the vibrational wave functions and the three parameters $\phi$, $\Delta Q_1''$, and $\Delta Q_2''$.

Equation 10b explains why the $\nu_3$ asymmetric stretch mode is inactive. The physical reason for $K_3 = 0$ is that since both initial and final states are symmetric ($C_{2v}$), there can be no net displacement in the $\nu_3$ asymmetric stretch coordinate between the states. Since the $\nu_3$ normal coordinate is the same for the two states, the integral in $Q_3$ factors out of the Franck–Condon overlap integral, eq 5, and is nonzero only for transitions between vibrational levels with both even or both odd wave functions, i.e., $\Delta v_3 = 0, \pm 2, \pm 4, \ldots$. Furthermore, the FCFs for $\Delta v_3 \neq 0$ are small because the corresponding wave functions would be orthogonal except that the frequencies and anharmonicities of the two states are different. Therefore, only the ($3_0^0$, $3_1^1$, $3_2^2$, ...) transitions have substantial FCFs. Finally, since excited anions ($v_3 \geq 1$) have small populations in the present work, only the $3_0^0$ origin transition is significant. Hence, we may neglect asymmetric stretch transitions entirely.

If Duschinsky rotation of the normal coordinates is neglected, $\phi = 0°$ and $\mathbf{J}'' = \mathbf{E}$, the unit matrix. In this special case, the parallel mode approximation, the overlap integral, eq 5, is separable into a product of integrals for each normal-coordinate dimension via eq 6, and the Franck–Condon factors for combination bands are given by the products of the corresponding overtone FCFs:

$$[C(v_1',v_2';v_1'',v_2'')]^2 = [C(v_1',0;v_1'',0)]^2[C(0,v_2';0,v_2'')]^2 \tag{11}$$

where we have excluded the asymmetric stretch mode. In the parallel mode approximation, only one-dimensional overlap integrals need to be calculated and the FCFs are determined by displacements in each normal coordinate.

The evaluation of the Franck–Condon integrals is carried out by the method of generating functions, which provides analytic expressions for the Franck–Condon factors. Hutchisson[41] developed this method for the case of harmonic or anharmonic oscillators in one dimension, and Sharp and Rosenstock[42] extended it to a multidimensional collection of harmonic oscillators. In the latter case, expressions for the Franck–Condon factors are obtained from the coefficients of a polynomial expansion derived from the generating functions. Sharp and Rosenstock[42] tabulated expressions for a few lower quantum levels. To obtain higher terms, we have performed the polynomial expansion using the MACSYMA[47] symbolic manipulation program, eliminating algebraic errors which plague the procedure otherwise.[42] MACSYMA also encodes the resulting expressions into FORTRAN. In an alternative procedure not used here, recurrence relations can be derived to obtain the Franck–Condon factors.[46,48]

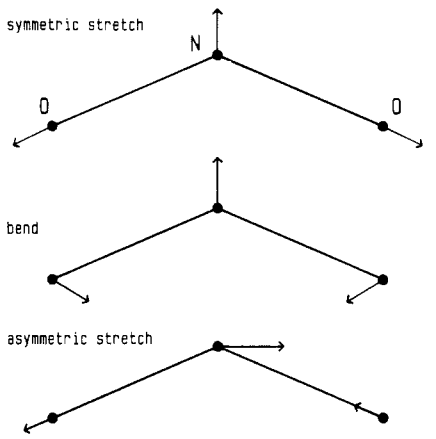


**Figure 4.** Normal modes of the $\nu_1$ (symmetric stretch), $\nu_2$ (bend), and $\nu_3$ (asymmetric stretch) vibrations of $NO_2$. The relative magnitudes of the normal-coordinate vectors are drawn to scale.

*2. Spectral Simulation.* The values of the geometry displacements are obtained by modeling the photoelectron spectrum. The relative intensities of vibrational transitions are given by

$$I(v_1',v_2';v_1'',v_2'') = \sigma_0[C(v_1',v_2';v_1'',v_2'')/C(0,0;0,0)]^2/\exp(G_0''/kT'') \tag{12}$$

where $\sigma_0$ is a scaling factor, $G_0''(v_1'',v_2'')$ is the vibrational energy of the anion, and $T''$ is the vibrational temperature of the anions. The peak positions are given by

$$\mathrm{eKE}(v_1',v_2';v_1'',v_2'') = h\nu - \mathrm{EA}(NO_2) - G_0'(v_1',v_2') + G_0''(v_1'',v_2'') \tag{13}$$

The vibrational energy $G_0'$ for $NO_2$ is calculated from the frequency and anharmonicity constants obtained above and listed in Table II, and $G_0''$ for $NO_2^-$ is obtained from the observed fundamental frequencies, neglecting anharmonicity. Each vibrational transition is convoluted with the rotational contour shown in the inset in Figure 3. A nonlinear least-squares optimization procedure is used to find the values of $\sigma_0$, $\Delta Q_1''$, and $\Delta Q_2''$ that give the best fit to the observed spectrum. Only the region above eKE = 0.5 eV is included in the fit because the instrumental sensitivity declines below that energy and because, according to ab initio calculations,[37] the $NO_2(A\ ^2B_2)$ excited state may be accessible below eKE = 0.33 eV. Fitting directly to the spectral data rather than to peak intensities avoids the problem of extracting intensities for partially unresolved transitions.

The two active vibrations of $NO_2$ are treated as uncoupled harmonic or anharmonic oscillators. The vibrational eigenmatrix $\mathbf{L}'$ for $NO_2$ is calculated by standard normal-coordinate analysis[49] from the harmonic valence force constants of Morino and Tanimoto[50] and the molecular geometry of Morina et al.[40] (see Table IV). Figure 4 displays vector diagrams for the three normal coordinates of $NO_2$. It is evident from Figure 4 that the $\nu_1$ symmetric stretch normal coordinate includes a substantial change in the molecular bond angle. Figure 4 also defines the conventions used for the signs of the normal-coordinate displacements.

The $\nu_1$ and $\nu_2$ modes of $NO_2^-$ are treated as two uncoupled harmonic oscillators, with the observed fundamental frequencies. Since most of the transitions originate in the ground state of the anion, neglect of its anharmonicity should not introduce significant errors. The force constants and geometry of gas phase $NO_2^-$ are not known experimentally, so we cannot directly determine its

(44) The choice of sign in eq 9 is dictated by the equivalent of eq 7 for the neutral molecule, $\mathbf{Q}' = \mathbf{J}'\mathbf{Q}'' + \mathbf{K}'$, where $\mathbf{J}' = \tilde{\mathbf{J}}'' = \tilde{\mathbf{L}}'\mathbf{L}''$.
(45) Eckart, C. *Phys. Rev.* **1935**, *47*, 552.
(46) Warshel, A.; Karplus, M. *Chem. Phys. Lett.* **1972**, *17*, 7.
(47) MACSYMA, Symbolics, Inc.
(48) Kupka, H.; Cribb, P. H. *J. Chem. Phys.* **1986**, *85*, 1303.
(49) Gwinn, W. D. *J. Chem. Phys.* **1971**, *55*, 477.
(50) Morino, Y.; Tanimoto, M. *J. Mol. Spectrosc.* **1986**, *115*, 442.

**TABLE V: Comparison of Franck–Condon Fits to Data**

| | method[a] | | | |
|---|---|---|---|---|
| | I | II | III | IV |
| Normal-Coordinate Displacements, amu$^{1/2}$ Å | | | | |
| $\mathbf{K}'' = \begin{pmatrix}\Delta Q_1''\\ \Delta Q_2''\end{pmatrix}$ | $\begin{pmatrix}-0.262\\ -0.544\end{pmatrix}$ | $\begin{pmatrix}-0.275\\ -0.566\end{pmatrix}$ | $\begin{pmatrix}-0.424\\ -0.407\end{pmatrix}$ | $\begin{pmatrix}-0.343\\ -0.487\end{pmatrix}$ |
| $\mathbf{K}' = \begin{pmatrix}\Delta Q_1'\\ \Delta Q_2'\end{pmatrix}$ | $\begin{pmatrix}+0.262\\ +0.544\end{pmatrix}$ | $\begin{pmatrix}+0.275\\ +0.566\end{pmatrix}$ | $\begin{pmatrix}+0.260\\ +0.526\end{pmatrix}$ | $\begin{pmatrix}+0.261\\ +0.536\end{pmatrix}$ |
| Normal-Coordinate Rotation | | | | |
| $\phi$, deg | 0 | 0 | −19.9 | −9 |
| Anion Geometry | | | | |
| $r''$, Å | 1.251 | 1.265 | 1.249 | 1.250 |
| $\alpha''$, deg | 117.1 | 116.4 | 117.6 | 117.5 |

[a] Model approximations (see text): I, harmonic oscillators; parallel modes. II, Morse oscillators; parallel modes. III, harmonic oscillators; $\phi$ from normal coordinates for crystalline $NO_2^-$. IV, harmonic oscillators; $\phi$ treated as adjustable parameters.

eigenmatrix $\mathbf{L}''$ in order to specify $\mathbf{J}''$ in eq 7 or, equivalently, $\phi$ in eq 10. Instead, we take four different approaches to specifying $\phi$ in the Franck–Condon calculations, described next. A comparison of the results will give an indication of the error produced by assumptions in the model.

In method I, we make the parallel mode approximation, i.e., $\phi = 0°$ and $\mathbf{J}'' = \mathbf{E}$. $NO_2$ is treated as a collection of harmonic oscillators. The Franck–Condon factors for overtone progressions are calculated by the one-dimensional Hutchisson method,[41] and combination band FCFs are given by eq 11. The least-squares fit to the data gives the values $|\Delta Q_1''| = 0.262$ and $|\Delta Q_2''| = 0.544$ for the displacement vector $\mathbf{K}''$ (all normal-coordinate displacements are given in units of amu$^{1/2}$ Å). The two possible directions for each normal-coordinate displacements are indistinguishable in the harmonic oscillator and parallel mode approximations, leading to four possible combinations.

In order to determine the changes in geometry in internal coordinates, we must first choose which normal-coordinate basis to use. Besides the fact that the normal coordinates for $NO_2^-$ are not known, the $NO_2$ normal-coordinate representation is the better choice because the vibrational transitions start in the ground state of $NO_2^-$ but end in high vibrational levels of $NO_2$. Therefore, we use the neutral's normal-coordinate displacements, $\mathbf{K}'$ from eq 9, to calculate the geometry changes via eq 8b. In the parallel mode approximation, the transformation is given simply by a change in sign. For the rest of the discussion, we will cite the displacements obtained from the least-squares fits in the $NO_2$ normal-coordinate basis, but both $\mathbf{K}''$ and $\mathbf{K}'$ are given in Table V.

Next we must determine the directions of the displacements. In accordance with the molecular orbital arguments discussed above, we choose the positive direction of $\Delta Q_2'$ since, as shown in Figure 4, that reduces the bond angle from $NO_2$ to $NO_2^-$. The positive direction of $\Delta Q_1'$ is chosen since that both increases the N–O bond length *and* decreases the bond angle. The resulting anion internal coordinates are $r'' = 1.251$ Å and $\alpha'' = 117.1°$. Taking the negative direction of $\Delta Q_1'$ instead would give $r'' = 1.135$ Å and $\alpha'' = 123.3°$. The change in $\alpha''$ for opposite directions of the symmetric stretch displacement indicates the amount of bend in that normal coordinate.

Method II is the same as method I except that anharmonicity is included in the $NO_2$ wave functions. The $\nu_1$ and $\nu_2$ modes are modeled by Morse oscillators. While the Morse function may not be a good approximation of the vibrational potentials (especially for the bend mode near linear configurations), our aim here is merely to estimate the effect of anharmonicity on the Franck–Condon analysis. The optimized displacements are $\Delta Q_1' = +0.275$ and $\Delta Q_2' = +0.566$, which gives $r'' = 1.265$ Å and $\alpha'' = 116.4°$. The anharmonicity means that the FCFs vary for different directions of the normal-coordinate displacements. A fit almost as good (the reduced sum of squared residuals, $\chi^2$, is just 4% larger) may be obtained with a different choice of directions of the displacements, $\Delta Q_1' = -0.259$ and $\Delta Q_2' = +0.567$, which gives $r'' = 1.136$ Å and $\alpha'' = 122.7°$. The difference in FCFs produced by the anharmonicity is not sufficient to allow us to distinguish experimentally between the directions of the displacements. Again, we take the positive displacements based on the molecular orbital considerations. The deviation between the anion geometries obtained by methods I and II, compared in Table V, gives a reasonable indication of the magnitude of the error produced by neglect of anharmonicity.

In method III, we include Duschinsky rotation by using the $NO_2^-$ vibrational eigenmatrix $\mathbf{L}''$ obtained from experimentally determined force constants for $NO_2^-$ in crystalline environments. Franck–Condon factors are calculated in the harmonic oscillator approximation by using the Sharp and Rosenstock method.[42] The frequencies for $NO_2^-$ in $NaNO_2$, in dilute concentrations in KBr crystals, and in aqueous solution are compared with the present gas-phase values in Table II. While we expect $NO_2^-$ in crystals to be perturbed compared to the gas phase, the frequency shifts are less than 5%, which indicates that the valence force fields might be similar. Also, the crystalline geometry[51] (Table IV) is close to that obtained for gas-phase $NO_2^-$ in methods I and II, above. Using the harmonic valence force constants of Kato and Rolfe[12] for $NO_2^-$ in crystalline KBr to determine $\mathbf{L}''$, we obtain $\phi = -19.9°$ for the rotation between normal coordinates. The photoelectron spectrum is fit by $\Delta Q_1' = +0.260$ and $\Delta Q_2' = +0.526$ (choosing the positive directions), which gives the anion geometry $r'' = 1.249$ Å and $\alpha'' = 117.6°$. When Duschinsky rotation is considered, the Franck–Condon factors for harmonic wavefunctions are identical for $\mathbf{K}' = -\mathbf{K}'$ but are different when just one element of $\mathbf{K}'$ ($\Delta Q_1'$ or $\Delta Q_2'$) is negated. Constraining the least-squares fit to negative values of $\Delta Q_1'$ gives an alternative fit of $\Delta Q_1' = -0.278$ and $\Delta Q_2' = +0.558$, or $r'' = 1.132$ Å and $\alpha'' = 123.3$. The latter fit is not as good as the former ($\chi^2$ is 70% larger), but it still fits the data within experimental uncertainty.

Finally, in method IV the rotation of the normal coordinates $\phi$ is treated as a adjustable parameter. As in method III, the vibrational modes of $NO_2$ are treated as harmonic oscillators. The best fit is obtained with $\phi = -9°$, $\Delta Q_1' = +0.261$, and $\Delta Q_2' = +0.536$. This gives an anion geometry of $r'' = 1.250$ Å and $\alpha'' = 117.5°$. The simulated spectrum for this method is compared with the experimental spectrum in Figure 3. Agreement with the observed intensities above 0.5 eV is excellent. All of the observed peaks are accounted for by overtones and combinations of the two active modes. Although method IV includes an additional adjustable parameter, the improvement in the overall fit to the data compared to methods I, II, and III is minor; i.e., all four fit the data within experimental uncertainties. We recommend the anion geometry values obtained by method IV, since it makes no prior assumptions about the $NO_2^-$ normal coordinates. The range of values obtained by the other methods, compared in Table V, provides a reasonable measure of possible errors due to model assumptions. Uncertainties due to the experimental uncertainties of the intensities and due to the least-squares fitting procedure itself are smaller. Our final estimate of the $NO_2^-$ anion geometry, with conservative uncertainties, is $r'' = 1.25 \pm 0.02$ Å and $\alpha'' = 117.5 \pm 2°$.

It is worth noting that the numerical values of the displacements in the $NO_2^-$ normal-coordinate basis, $\mathbf{K}''$, vary to a much greater extent for the fits to the data for different $\phi$ than do those in the $NO_2$ basis, $\mathbf{K}'$. $\mathbf{K}''$ and $\mathbf{K}'$ are compared in Table V. This result supports the qualitative conclusion, above, that it is more accurate to use the final-state normal coordinates to calculate changes in the internal geometry, when the parallel mode approximation is to be used. As Coon et al.[52] have discussed, the parallel mode approximation becomes exact for the special case where the vibrational wave functions of the initial state are spherically symmetric in normal-coordinate space (e.g., if all modes are harmonic and have the same frequency), and the final-state normal coordinates are used for the displacements.

As a final test of the assignment of the origin, we attempted Franck–Condon fits to the data with the origin shifted by one or

(51) Kay, M. I.; Frazer, B. C. *Acta Crystallogr.* **1961**, *14*, 56.
(52) Coon, J. B.; DeWames, R. E.; Loyd, C. M. *J. Mol. Spectrosc.* **1962**, *8*, 285.

two quanta of the bend or stretch. With these assignments, it was impossible to reproduce all of the peak intensities within the uncertainties of the experiment. Thus, the assignment of the vibrational origin is unambiguously confirmed.

*C. Comparison with Previous Experiments and Theory.* Table IV compares the present result with other experimental and theoretical molecular geometries for $NO_2^-$. Ab initio self-consistent-field (SCF) calculations for $NO_2^-$ give bond lengths in the range 1.22-1.26 Å and bond angles of 117-118°. These values agree well with the present results. The geometric constants of $NO_2^-$ in crystalline environments differ from our determination for gas-phase $NO_2^-$ by only a few percent. This result is consistent with the ab initio results of Goddard and Klein,[16] who calculated the structure of $NO_2^-$ interacting with one or two sodium ions and found only modest changes in the $NO_2^-$ geometry. Ozone, which is isoelectronic with $NO_2^-$, has a bond length of 1.278 Å and a bond angle of 116.8°,[53] quite close to the geometry found for here for $NO_2^-$.

Our conclusions regarding the anion geometry suggest a reinterpretation of the results of Woo et al.[5] They modeled photodetachment threshold data for $NO_2^-$ at photon energies up to 2.8 eV using a Franck-Condon analysis, in which the Franck-Condon intensities were derived from the increase in the photodetachment cross section at the threshold for each transition. The magnitude and behavior of the photodetachment cross section beyond the threshold region were fixed by a fit to their data in the ultraviolet, 3.5-4.8 eV. Woo et al. found two possible fits, $r'' = 1.25$ Å, $\alpha'' = 116°$ and $r'' = 1.15$ Å, $\alpha'' = 119.5°$, corresponding to opposite directions of the displacement in the $\nu_1$ symmetric stretch normal coordinate. The latter geometry gave a better least-squares fit to the threshold data (by a factor of 10 in the sum of squared residuals of Franck-Condon factors), and it was chosen by Woo et al. primarily on that basis. Our observations provide intensities for individual transitions directly, which should be more sensitive to small difference in Franck-Condon intensities than threshold measurements, and we also observe higher vibrational transitions. We find no direct experimental basis for determing the direction of the geometry displacements. We believe the molecular orbital considerations and comparisons to ab initio calculations, above, argue convincingly in favor of the configuration with longer bond length and smaller bond angle. In particular, it seems unlikely that the SCF calculations of the bond lengths (Table IV) are in error by 0.07-0.11 Å (6-10%). Therefore, we suggest a reinterpretation of the data of Woo et al. in favor of their alternative $NO_2^-$ geometry ($r'' = 1.25$ Å, $\alpha'' = 116°$), which agrees well with the present work and with theoretical values. A possible source of the discrepancy is photodetachment to electronically excited states of $NO_2$ at the higher photon energies in the study of Woo et al., which could alter the shape and magnitude of the cross section and therefore the fitting parameters used for the threshold data.

(53) Herzberg, G. *Molecular Spectra and Molecular Structure. III. Electronic Spectra and Electronic Structure of Polyatomic Molecules*; Van Nostrand Reinhold: New York, 1966; p 604.

## V. Conclusion

We have measured the 351-nm photoelectron spectrum of $NO_2^-$. The electron affinity of $NO_2$ is 2.273 ± 0.005 eV.

The vibrational spectrum of the ground electronic state of $NO_2$ is observed within 1 eV of its ground vibrational state. There is no evidence of electronic excited states in this region. In contrast to the highly complicated visible spectrum of $NO_2$, the vibrational structure in the energy range studied here is completely described by simple overtone and combination progressions in the two totally symmetric vibrational modes of the ground electronic state. Franck-Condon analysis of the vibrational band intensities provides an estimate of the molecular geometry of the anion: $r'' = 1.25 \pm 0.02$ Å and $\alpha'' = 117.5 \pm 2°$ for $NO_2^-$, compared to $r' = 1.194$ Å and $\alpha' = 133.9°$ for $NO_2$.[40] The large increase in the bond angle upon removal of an electron from $NO_2^-$ is responsible for the extended progression observed in the bend vibrational mode. The symmetric stretch progression is also active due to a decrease in the N-O bond length from $NO_2^-$ to $NO_2$.

*Acknowledgment.* We thank Dr. Keith Lykke for his expert work on the design and development of the ultraviolet laser system. We are grateful for helpful discussions with Dr. S. V. ONeil, Professor G. Barney Ellison, and Dr. Sean Moran. This research is supported by National Science Foundation Grants CHE 83-16028 and PHY 86-04508.

**Registry No.** $NO_2^-$, 14797-65-0.

# Unimolecular Reaction Rate Theory for Highly Flexible Transition States. 2. Conventional Coordinate Formulas for the Various Possible Fragment Combinations. Miscellaneous Topics

**Stephen J. Klippenstein and R. A. Marcus***

*Arthur Amos Noyes Laboratory of Chemical Physics, California Institute of Technology,† Pasadena, California 91125* *(Received: January 26, 1988; In Final Form: March 30, 1988)*

A method for using conventional coordinates in the implementation of RRKM theory for unimolecular dissociations was described in part 1 of this series, for the case where both fragment molecules are nonlinear. The corresponding formalism for all possible types of fragments, atomic, linear, and nonlinear fragments and their combinations, is presented here. Also discussed analytically is the tendency, in a unimolecular dissociation, for the position of the transition state to move to shorter fragment-fragment separation distances with increasing total energy $E$. This tendency has marked consequences, including increasing deviation of rate constants from those of phase space theory with increasing $E$ and, in the case of fragment-fragment recombination, a corresponding tendency for high-pressure rate constants to decrease with increasing temperature. Two other topics considered in this paper are the case of two minima in the variational calculation and the role of the repulsive potential energy curves in the unimolecular dissociations under consideration.

## I. Introduction

The number of states $N_{EJ}(R)$ for a given excess energy $E$, total angular momentum quantum number $J$, and position $R$ along a reaction coordinate enters into the RRKM theory[1] of unimolecular dissociations. With a sufficiently accurate determination of this quantity and of the density of states $\rho_{EJ}$ of the molecule itself, good agreement between theoretically and experimentally de-

† Contribution No. 7731. Dedicated to the memory of Ed Lee, whose joyous spirit in research will always be remembered.

(1) Robinson, P. J.; Holbrook, K. A. *Unimolecular Reactions*; Wiley: New York, 1972. Forst, W. *Theory of Unimolecular Reactions*; Academic: New York, 1973. Weston, R. E.; Schwarz, H. A. *Chemical Kinetics*; Prentice-Hall: Englewood Cliffs, NJ, 1972. Marcus, R. A. *J. Chem. Phys.* **1952**, *20*, 359. Marcus, R. A.; Rice, O. K. *J. Phys. Colloid Chem.* **1951**, *55*, 894. Marcus, R. A. *J. Chem. Phys.* **1965**, *43*, 2658; **1970**, *52*, 1018.

0022-3654/88/2092-5412$01.50/0 